PHYSICAL REVIEW B **96**, 081115(R) (2017)

Ab initio calculation of spin-orbit coupling for an NV center in diamond exhibiting dynamic Jahn-Teller effect

Gergő Thiering[1] and Adam Gali[1,2,*]

[1]*Wigner Research Centre for Physics, Hungarian Academy of Sciences, PO Box 49, H-1525 Budapest, Hungary*

[2]*Department of Atomic Physics, Budapest University of Technology and Economics, Budafoki út 8, H-1111 Budapest, Hungary*

(Received 20 June 2017; published 24 August 2017)

Point defects in solids may realize solid state quantum bits. The spin-orbit coupling in these point defects plays a key role in the magneto-optical properties that determine the conditions of quantum bit operation. However, experimental data and methods do not directly yield these highly important data, particularly for such complex systems where the dynamic Jahn-Teller (DJT) effect damps the spin-orbit interaction. Here, we show for an exemplary quantum bit, the nitrogen-vacancy (NV) center in diamond, that *ab initio* supercell density functional theory provides a quantitative prediction for the spin-orbit coupling damped by DJT. We show that DJT is responsible for the multiple intersystem crossing rates of the NV center at cryogenic temperatures. Our results pave the way toward optimizing solid state quantum bits for quantum information processing and metrology applications.

DOI: 10.1103/PhysRevB.96.081115

Dopants in solids are promising candidates for implementations of quantum bits for quantum computing [1,2]. In particular, the negatively charged nitrogen-vacancy defect (NV center) in diamond [3] has become a leading contender in solid state quantum information processing because of its long spin coherence time (up to several milliseconds in ultrapure diamonds [4]) and ease of optical initialization and readout of spin state [5], even nondestructively [6,7]. The NV center consists of a nitrogen atom substituting a carbon atom in the diamond lattice adjacent to a vacancy with forming a C_{3v} symmetry that dictates the selection rules for the magneto-optical processes [Fig. 1(a)]. The geometry and the electronic structure of the NV center in diamond have been discussed previously based on highly converged *ab initio* plane-wave large-supercell calculations [8,9]. The defect exhibits a fully occupied lower a_1 level and a double-degenerate upper e level filled by two parallel-spin electrons in the gap comprising an $S = 1$ high-spin ground state [Fig. 1(b)]. The high-spin ^3E excited state can be well described by promoting an electron from the lower defect level to the upper level in the gap [10]. Between excited state and ground state triplets dark singlets appear that can selectively flip $m_s = \pm 1$ states to $m_s = 0$ states in the optical excitation cycle [11–15]; i.e., the electron spin can be spin polarized optically [Fig. 1(c)]. The spin-selective decay is predominantly caused by the intersystem crossing (ISC) between the optically accessible triplet ^3E excited state [see Fig. 1(c)] and the singlet $^1A_1$ state which is mediated by the spin-orbit coupling between these states and phonons [14,15]. Generally, the spin-orbit coupling plays a crucial role in the optical spin polarization and readout of the NV quantum bit (qubit) and alike [16–20].

The strength of the spin-orbit coupling in the NV center may be detected at low-temperature photoluminescence excitation (PLE) measurements of the ^3E excited state in high-quality diamond samples [21] where the strain does not deteriorate the fine spin level structure of the ^3E excited state [14]. By combining the PLE data and group theory analysis, the spin-orbit strength was estimated to be 5.33 ± 0.03 GHz [21,22] recorded at $T < 20$ K. We note that additional splitting and shift of the levels appears due to electron-spin–electron-spin interaction [14] that is not discussed further here. Regarding the spin-orbit mediated ISC process, three different ISC rates have been recently deduced in the experiments [23]. This is surprising because group theory [14] predicts only a single decay channel from the A_1 substate of the ^3E triplet. This phenomenon was qualitatively explained by assuming weak coupling of symmetry-breaking acoustic e phonons to the A_1, $E_{1,2}$, and A_2 substates that was derived in the frame of perturbation theory of electron-phonon coupling [23,24]. Nevertheless, this theory does not quantitatively account for the experimental ratio between the ISC rates at cryogenic temperature.

Deep understanding of the nature of ^3E excited state might resolve this issue. *Ab initio* simulations [25] and experiments [26–28] imply that the ^3E excited state exhibits the dynamic Jahn-Teller (DJT) effect where the vibronic levels split in the 10 meV region [25]. This is more than three orders of magnitude larger than the observed spin-orbit coupling; thus spin-orbit coupling can be considered as a perturbation with respect to the DJT effect. In DJT systems, the phonons and orbitals are strongly coupled which goes *beyond* the perturbation theory of electron-phonon coupling. That may lead to the damping or even quenching of spin-orbit coupling [29] where the damping parameter, i.e., the Ham reduction factor, depends on the strength of electron-phonon coupling. For this reason, the strength of the intrinsic spin-orbit coupling in the NV center is still an open question. In addition, the presumably strong electron-phonon coupling in the ^3E state may have implications in the ISC process of the NV center.

Here we show by *ab initio* supercell density functional theory (DFT) calculations that the intrinsic spin-orbit coupling together with the damping caused by the DJT can be accurately predicted for the NV center in diamond. We show that strong electron-phonon coupling in the triplet excited state is an important aspect of the theory of nonradiative decay in the NV center and that this theory accurately reproduces the ratio between the experimental ISC rates.

*gali.adam@wigner.mta.hu

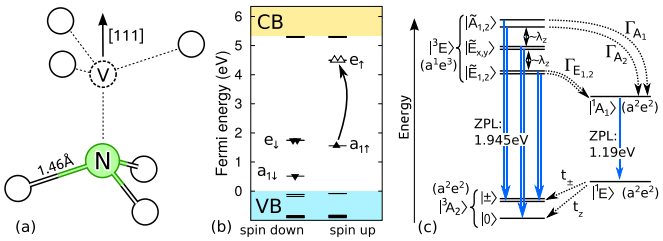

FIG. 1. NV center in diamond. (a) Schematic diagram of the structure of the negatively charged defect with the optimized carbon-nitrogen bond length. The symmetry axis of the defect in the diamond lattice is shown. (b) The calculated defect levels in the gap are depicted in the ground state where the curved arrow symbolizes the ΔSCF procedure for creating the triplet excited state. The e states are double degenerate. VB and CB correspond to valence and conduction bands, respectively. (c) The corresponding ground state and excited states are shown as well as the optical electron spin polarization cycle. The spin-orbit splitting λ_z is depicted that separates the sublevels in the triplet ^3E excited state. The corresponding intersystem crossing rates between the ^3E substates ($\tilde{A}_{1,2}$, $\tilde{E}_{1,2}$ double group representations) and the singlet $^1A_1$ are labeled by Γs. The tilde labels the vibronic nature of these states. The intersystem crossing ($t_\pm$ and t_z) from the ^1E to the triplet ground state is shown for the sake of completeness and closes the spin polarization cycle.

We apply the supercell plane-wave spin-polarized DFT method to model the defect with the usual Born-Oppenheimer approximation. The Born-Oppenheimer approximation treats the nuclei or ions as classical particles, where the motions of the electrons are solved in fixed coordinates of these ions providing the total energy of the system parametrized by the coordinates of ions. By varying the coordinates of ions one can achieve an adiabatic potential energy surface (APES) map of the system. The global minimum of the APES defines the optimized geometry of the system. The NV center was modeled mostly in a 512-atom cubic supercell within the Γ-point approximation that provides convergent electron charge density. In our simulations, we apply the VASP 5.4.1 plane-wave code [30] within the projector-augmented wave method (PAW) [31,32] to treat the ions. We utilize the standard PAW potentials and a convergent plane-wave cutoff of 370 eV. We apply a very stringent upper limit of 10^{-4} eV/Å for the forces in the geometry optimization. For the calculation of the phonon spectrum we generate the dynamical matrix via finite differences of total energies. We applied the Huang-Rhys theory to calculate the overlap of phonon states [33,34]. The implementation is described in our previous publication [35]. The ^3E state is calculated by the constrained-occupation DFT method by following the picture in Fig. 1(b) (ΔSCF) [10]. The singlet states cannot be described properly by conventional Kohn-Sham density functional theory because of the high correlation between the e orbitals. A crude estimation of the $^1A_1$ state is to apply a spin-polarized singlet occupation of the e_x orbital. We use this method to estimate the geometry of $^1A_1$ needed in the description of ISC. The optimized geometry in the excited state is calculated by minimizing the forces acting on the atoms in the electronic excited state within the ΔSCF procedure. The electronic structure is calculated using the HSE06 hybrid functional [36,37] within DFT. Using this technique, it is possible, in particular, to reproduce the experimental band gap and the charge transition levels in group-IV semiconductors within 0.1 eV accuracy [38].

The spin-orbit coupling (SOC) was calculated within the noncollinear approach as implemented in VASP 5.4.1 (see Ref. [39]). In our particular cases, the C_3 axis of the defect sets the quantization axis of the spin that fixed in the calculation. As SOC is a tiny perturbation to the system we also fixed the coordinates in SOC calculations as obtained from the spin-polarized DFT calculations. Direct comparison to the experimental data can be extracted from the z component of SOC which coincides with the quantization axis of the spin; thus it is the diagonal term in the matrix elements representing the different components of SOC. The spin-orbit scattering rate, however, can be calculated from the $\lambda_\perp$ components that are off-diagonal terms in the SOC Hamiltonian. SOC was calculated in the high-symmetry configurations of the NV(−) center. In this case, a single electron should occupy the double-degenerate Kohn-Sham e state in the spin minority channel. After applying SOC this double-degenerate Kohn-Sham state will split into e_x and e_y states. By using the ΔSCF procedure it is feasible either to occupy the e_x or e_y state, and the calculated total energy difference is the strength of SOC. We find that half of this total energy difference is equal within 10^{-7} eV to the split of e_x and e_y Kohn-Sham levels when these two states are occupied by half-half electrons. Thus, the strength of SOC can be calculated by the half-half occupation of the e states following the SOC splitting of these e states. It is crucial to use the Γ-point approximation in the integration of the Brillouin zone in this procedure because the degenerate e orbitals slightly split in other k points by reducing the symmetry of the orbitals that makes the readout of the SOC parameters ambiguous. We further note that $\langle {}^3E(A_1)|H_{\rm SO}|{}^3E(A_1)\rangle = \frac{1}{2}\langle e_+|H_{\rm SO}|e_+\rangle$ and $\langle {}^3E|H_{\rm SO}|{}^1A_1\rangle = \frac{1}{\sqrt{2}}\langle e_+^\downarrow|H_{\rm SO}|a_1^\uparrow\rangle$ for the NV(−) defect where the latter is valid with the two basic assumptions described below in the discussion of ISC rates. Here the arrows represent the corresponding spin states and $|e_\pm\rangle = \frac{1}{\sqrt{2}}(|e_x\rangle \pm i|e_y\rangle)$. We note that we calculated SOC with the Perdew-Burke-Ernzerhof (PBE) DFT functional [40] too for test purposes which is a significantly faster method than the HSE06 DFT method. In that case we used PBE-optimized lattice constants and defect geometries.

First, we consider the spin-orbit splitting λ_z. Batalov and co-workers deduced a value of 5.3 GHz for this spin-orbit coupling (SOC) from PLE measurements [21] observed at 6 K. We study this interaction with our *ab initio* method. The convergent SOC was achieved with scaling supercell size up to 1000 atoms in the hybrid functional calculations and applying an exponential fit to the calculated results (see Ref. [34]). The calculated λ_z for the ^3E state of NV(−) is 15.8 GHz which is about 3× larger than the measured one. However, the ^3E excited state is principally Jahn-Teller unstable in the high C_{3v} symmetry that can lead to partial or full quenching of the spin-orbit coupling [29].

We conclude that the spin-orbit coupling should be studied *beyond* the Born-Oppenheimer approximation. The ^3E state is orbitally degenerate where a symmetry breaking e phonon or quasilocal vibration mode can drive out the system from the high symmetry that may couple the components of the

double-degenerate E electron wave functions. This is the so-called $E \otimes e$ DJT system that was already analyzed in detail by Ham [41] and Bersuker [42,43]. Here, since the defect has C_{3v} symmetry the quadratic JT Hamiltonian should be considered (see the analysis in Ref. [34]). By introducing the dimensionless coordinates along $x = a_x^\dagger + a_x$ and $y = a_y^\dagger + a_y$, the quadratic DJT Hamiltonian reads as

$$\hat{H} = \hbar\omega_e(a_x^\dagger a_x + a_y^\dagger a_y + 1) + F(x\sigma_z + y\sigma_x) + G[(x^2 - y^2)\sigma_z + 2xy\sigma_x], \quad (1)$$

where $a_{x,y}$, $a_{x,y}^\dagger$ operators create or annihilate an e vibration. The double-degenerate e mode has x and y components. $\hbar\omega_e$ is the energy of the effective e mode that drives the distortion of the system, and F and G are electron-vibration coupling related terms. The electrons are represented by the Pauli matrices σ. F and G can be directly derived from the calculated APES which results in the Jahn-Teller energy ($E_{\rm JT}$) and the barrier energy $\delta_{\rm JT}$ between the global minima (see Fig. 2) as follows: $E_{\rm JT} = \frac{F^2}{2\hbar\omega_e}$, $G = \delta_{\rm JT}\hbar\omega_e/2E_{\rm JT}$. The $\hbar\omega_e$ energy can be derived from the parabola fitting to the calculated APES. Finally, all the parameters can be readout from APES (see Table I) which allows us to solve Eq. (1) numerically, which provides the electron-phonon coupling coefficients [34]. The exact solution can be expanded into series as $|\Psi_\pm\rangle = \sum_{nm}[c_{nm}|E_\pm\rangle \otimes |n,m\rangle + d_{nm}|E_\mp\rangle \otimes |n,m\rangle]$, where we limit the expansion up to four oscillator quanta ($n + m \leqslant 4$) which is numerically convergent within 0.2%. The p reduction factor that reduces the spin-orbit interaction can then be calculated from these coupling coefficients as $p = \sum_{nm}[c_{nm}^2 - d_{nm}^2]$ which represents the mixture of the E^+ component with the E^- component of the ^3E, which results in the quenching of the effective angular momentum. We note that taking only the linear term either numerically or approximately [41] results in 10% lower value for the damping factor (see details in Ref. [34]).

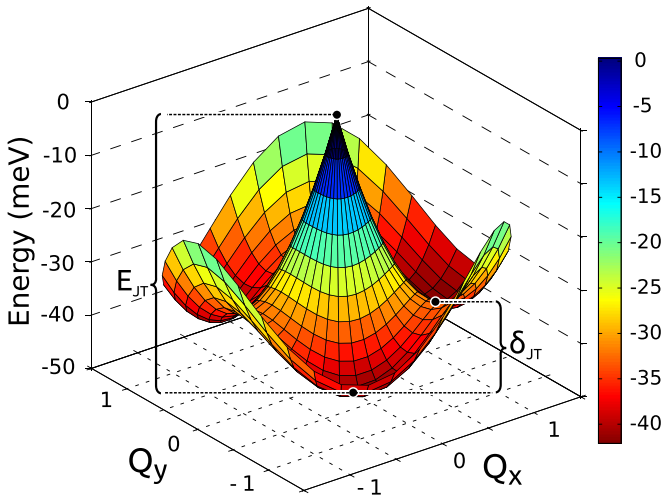

FIG. 2. Adiabatic potential surface (APES) of the quadratic DJT system for NV(−) ^3E excited state. $Q_{x,y}$ configuration coordinates represent the degenerate e phonon. $E_{\rm JT}$ is the Jahn-Teller energy which is the energy difference between the total energy at the high-symmetry configuration and the distorted configuration. The energy barrier of $\delta_{\rm JT}$ occurs between the three equivalent distorted configurations.

TABLE I. SOC splitting parameters for the excited state of NV(−). By using $E_{\rm JT}$ Jahn-Teller energy, $\hbar\omega_e$ phonon energy, and $\delta_{\rm JT}$ barrier energy the p reduction factors can be evaluated. The partially quenched $p\lambda_z$ SOC parameters are expected to be observed in the experiments. The calculated values are valid at 0 K. We note that the PBE functional results in $E_{\rm JT} = 25$ meV and $\delta_{\rm JT} = 10$ meV (see Ref. [25]).

λ_z (GHz)	$E_{\rm JT}$ (meV)	$\delta_{\rm JT}$ (meV)	$\hbar\omega_e$ (meV)	p	$p\lambda_z$ (GHz)	Exp. (GHz)
15.8	41.8	9.1	77.6	0.304	4.8	5.3[a], 5.33 ± 0.03[b]

[a] λ_z in Ref. [21] measured at 6 K.
[b] λ_z in Ref. [22] observed below 20 K.

The calculated quenching factor is large which can strongly modify the intrinsic (purely orbital) value. The final result is 4.8 GHz which agrees within 10% with the experimental result (see Table I). Despite the remaining discrepancy between the calculated and measured SOC, the improvement is enormous in SOC when the DJT effect is considered which demonstrates the complex physics of this system. We emphasize that this result was obtained from first-principles calculations in the micro-electron-volt energy region of SOC.

We turn to the investigation of the ISC process which depends on the perpendicular component of the spin-orbit coupling, $\lambda_\perp$ [14,15]. The ISC rate between the triplet ^3E and $^1A_1$ may be calculated [23] as

$$\Gamma_{A_1} = 4\pi\hbar\lambda_\perp^2 F(\Delta), \quad (2)$$

where $\lambda_\perp$ is given in rad/s units and F is the energy-dependent density of states multiplied by the overlap of the vibrational states of ^3E and $^1A_1$ electronic states, and Δ is the energy gap between ^3E and $^1A_1$ states. Here, we follow the convention in Ref. [23] for the definition of $\lambda_\perp$. We note that Eq. (2) implicitly assumes that the electronic states of ^3E and $^1A_1$ participating in the ISC process do not change their character during the motion of nuclei; i.e., the $\lambda_\perp$ remains fixed independently of the coordinates of the atoms. This assumption is an analog to the Condon approximation on the optical excitation of polyatomic systems that we call basic assumption (i). This theory can explain the ISC process from the A_1 state.

We demonstrate below that by invoking the DJT nature of the ^3E triplet state, the three ISC rates at cryogenic temperatures [23,24] can be naturally explained. To this end, we express the four $m_s = \pm 1$ electron-phonon coupled ^3E wave functions in the Born-Oppenheimer basis of symmetry-adapted terms, $|\tilde{A}_1\rangle$, $|\tilde{A}_2\rangle$, $|\tilde{E}_1\rangle$, $|\tilde{E}_2\rangle$ (see Supplemental Material [34]). The symmetry-adapted basis allows us to determine the phonon-induced or DJT-induced mixing of electronic orbitals between the $m_s = \pm 1$ states. One can realize that degenerate $|\tilde{E}_1\rangle$ and $|\tilde{E}_2\rangle$, and $|\tilde{A}_2\rangle$ vibronic wave functions contain the $|A_1\rangle$ electronic orbital which makes the spin-orbit mediated scattering to the $^1A_1$ singlet state feasible. This explains the three different ISC rates even at cryogenic temperature. By taking the vibronic nature of these $m_s = \pm 1$ states

into account, the corresponding ISC rates can be written as

$$\Gamma_{A_1} = 4\pi\hbar\lambda_\perp^2 \sum_{i=1}^{\infty} \left[c_i^2 F(\Delta - n_i\hbar\omega_e)\right], \quad (3)$$

$$\Gamma_{E_{12}} = 4\pi\hbar\lambda_\perp^2 \sum_{i=1}^{\infty} \left[\frac{d_i^2}{2} F(\Delta - n_i\hbar\omega_e)\right], \quad (4)$$

$$\Gamma_{A_2} = 4\pi\hbar\lambda_\perp^2 \sum_{i=1}^{\infty} \left[f_i^2 F(\Delta - n_i\hbar\omega_e)\right], \quad (5)$$

where c_i, d_i, and f_i expansion coefficients are calculated *ab initio* by solving the electron-phonon Hamiltonian, and n_i is the quantum number of the phonons of the $^1A_1$ electronic state.

Here, we still applied the basic assumption (i) in the ISC process but we explicitly consider the DJT nature of the ^3E state. We found that f_i^2 is very small (see Supplemental Material [34]); thus Γ_{A_2} is two orders of magnitude smaller than Γ_{A_1} or $\Gamma_{E_{1,2}}$, in agreement with the experiment. The ratio of $\Gamma_{E_{1,2}}/\Gamma_{A_1}$ requires the explicit calculation of the F function that depends on Δ and the overlap of phonon states of the electronic states. As the value of Δ is unknown we use it as a parameter. The theoretical upper limit of Δ can be calculated from the zero-phonon line (ZPL) energies of the visible and near-infrared (NIR) optical transitions [44] which results in $\Delta < 0.75$ eV, which ensures that the ^1E singlet level is above that of the $^3A_2$ ground state. Regarding the overlap of phonon states, we apply the Huang-Rhys approximation to calculate this quantity which is within our assumption (i) but further assumes the parabolic APES of the electronic states so the phonon energies and states are the same in the two electronic states involved in ISC. This Huang-Rhys approximation was already implicitly employed by using ω_e in Eqs. (3)–(5) where the value $\hbar\omega_e$ can be read in Table I. As the ISC occurs between ^3E and $^1A_1$ states, the optimized geometry of these states is required in the calculation of their phonon overlap function that is characterized by its S Huang-Rhys factor (see Supplementary Material [34]). However, the Kohn-Sham HSE06 DFT cannot explicitly calculate the $^1A_1$ state. An upper bound theoretical limit on the S factor can be taken from the geometry change between the $^3A_2$ ground state and ^3E excited state where the DJT feature in ^3E geometry should be eliminated. Our calculated S factor for this optical transition agrees well with the value deduced from the experimental PL spectrum of NV(−) [see Fig. 3(b)] which confirms the accuracy of our *ab initio* approach [45]. By eliminating the DJT feature in the phonon overlap function, we find $S = 3.11$ [see Fig. 3(c)]. By assuming that the geometries of the $^3A_2$ ground state and the $^1A_1$ singlet are the same because of sharing the same e^2 electronic configuration, $S = 3.11$ can be a theoretical upper bound limit. However, sharing the same e^2 electronic configuration does not guarantee the same optimized geometries for $^3A_2$, and $^1A_1$ and ^1E singlets. Indeed, NIR PL and absorption studies found $S = 0.9$ for the $^1A_1 \leftrightarrow {}^1E$ optical transition in NV(−) [44]; thus the geometries of the two singlets differ. We conclude that it is not well supported to assume that the geometries of $^1A_1$ and $^3A_2$ are exactly the same. Therefore, we roughly approximate the geometry of the $^1A_1$ state from the $(e_x e_x)$ singlet spin-polarized HSE06 DFT calculation. We find $S = 2.61$ with this procedure which reflects a small change in the geometry [see Fig. 3(c)]. The final result on the ratio of $\Gamma_{E_{1,2}}/\Gamma_{A_1}$ as a function of Δ is plotted in Fig. 3(a). As can be seen the $S = 3.11$ curve implies too large Δ values going above the theoretical upper limit in a wide region when the experimental ratio is reproduced. On the other hand, the $S = 2.61$ curve mostly provides reasonable Δ values. This implies that S should be indeed significantly smaller than that of $S = 3.11$ derived from the ground state geometry.

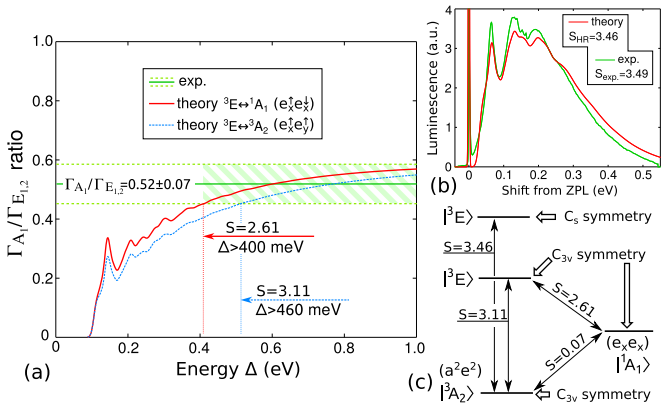

FIG. 3. The DJT theory of ISC rates on NV(−) center. (a) The measured ratio of ISC rates (straight horizontal line) with the given error bar (dotted horizontal lines) from Ref. [23] and the calculated ISC rates as a function of Δ with two S parameters that are derived from two geometry changes as explained in the legend and panel (c). (b) The experimental [44] and our *ab initio* simulated PL spectrum where S_{exp} and S_{HR} are the experimentally deduced and calculated Huang-Rhys factors. The contribution of ZPL (sharp peak) to the full PL spectrum is about 4%. (c) Diagram of the calculated S factors. The energy levels are not scaled for the sake of clarity. The geometry of the $^1A_1$ singlet is approximated from that of the $(e_x e_x)$ singlet determinant.

In order to calculate the ISC rates, $\lambda_\perp$ should be determined. Unlike the case of λ_z, one has to apply an approximation to do this, namely, that the Kohn-Sham wave functions building up the ^3E state and the $^1A_1$ multiplet do not change. This is basic assumption (ii) in the ISC rate calculation which permits us to compute $\lambda_\perp$ *ab initio* by using the a_1 and $e_{x,y}$ Kohn-Sham wave functions of the NV(−) in the ^3E excited state [see Fig. 1(b)]. The converged intrinsic value is $\lambda_\perp = 56.3$ GHz which is relatively large, and it is not damped by the DJT because the $^1A_1$ state is not part of the DJT effect. We note that the nitrogen contribution is minor in λ_z whereas it is significant in $\lambda_\perp$ which explains the large anisotropy between λ_z and $\lambda_\perp$. With these $\lambda_\perp$, S factors and reasonable Δ values in Fig. 3(a), we obtain ISC rates an order of magnitude larger than the experimental ones at $\Gamma_{A_1} = 16.0$ MHz and $\Gamma_{E_{1,2}} = 8.3$ MHz [23]. We conclude that $\lambda_\perp$ might be too large. We suspect that the large $\lambda_\perp$ is a consequence of the two basic assumptions, particularly, of assumption (ii). The exact determination of Δ and $\lambda_\perp$ requires an accurate *ab initio* calculation of the $^1A_1$ multiplet state as a function of the configuration coordinate of the NV(−) center. That would make possible a full *ab initio* calculation of the ISC rates. Finally, we emphasize here that the ratio of the low-temperature multiple ISC rates is quantitatively reproduced by our DJT theory.

In conclusion, we demonstrated on the NV center in diamond that the spin-orbit coupling can be well calculated from *ab initio* methods in dynamic Jahn-Teller systems. We implemented and applied a method to calculate the damping factor on spin-orbit coupling caused by the DJT effect from first principles. Our theory revealed that the strong coupling between electrons and phonons is responsible for the multiple scattering rates at cryogenic temperatures. Our results demonstrate the power of *ab initio* modeling of this complex system that can be applied to other solid state qubits, in order to predict their key properties (electron-phonon coupling and spin-orbit coupling) that determine their initialization and readout.

Support from the EU Commission (DIADEMS Project Contract No. 611143) is acknowledged.

[1] T. D. Ladd, F. Jelezko, R. Laflamme, Y. Nakamura, C. Monroe, and J. L. O'Brien, Nature (London) **464**, 45 (2010).
[2] D. D. Awschalom, L. C. Bassett, A. S. Dzurak, E. L. Hu, and J. R. Petta, Science **339**, 1174 (2013).
[3] L. du Preez, Ph.D. thesis, University of Witwatersrand, 1965.
[4] G. Balasubramanian, P. Neumann, D. Twitchen, M. Markham, R. Kolesov, N. Mizuochi, J. Isoya, J. Achard, J. Beck, J. Tissler, V. Jacques, P. R. Hemmer, F. Jelezko, and J. Wrachtrup, Nat. Mater. **8**, 383 (2009).
[5] F. Jelezko and J. Wrachtrup, Phys. Status Solidi A **203**, 3207 (2006).
[6] B. B. Buckley, G. D. Fuchs, L. C. Bassett, and D. D. Awschalom, Science **330**, 1212 (2010).
[7] L. Robledo, L. Childress, H. Bernien, B. Hensen, P. F. A. Alkemade, and R. Hanson, Nature (London) **477**, 574 (2011).
[8] A. Gali, M. Fyta, and E. Kaxiras, Phys. Rev. B **77**, 155206 (2008).
[9] A. Gali, Phys. Rev. B **80**, 241204 (2009).
[10] A. Gali, E. Janzén, P. Deák, G. Kresse, and E. Kaxiras, Phys. Rev. Lett. **103**, 186404 (2009).
[11] J. Harrison, M. Sellars, and N. Manson, Diam. Relat. Mater. **15**, 586 (2006).
[12] J. Wrachtrup and F. Jelezko, J. Phys.: Condens. Matter **18**, S807 (2006).
[13] N. B. Manson, J. P. Harrison, and M. J. Sellars, Phys. Rev. B **74**, 104303 (2006).
[14] J. R. Maze, A. Gali, E. Togan, Y. Chu, A. Trifonov, E. Kaxiras, and M. D. Lukin, New J. Phys. **13**, 025025 (2011).
[15] M. W. Doherty, N. B. Manson, P. Delaney, and L. C. L. Hollenberg, New J. Phys. **13**, 025019 (2011).
[16] C. Hepp, T. Müller, V. Waselowski, J. N. Becker, B. Pingault, H. Sternschulte, D. Steinmüller-Nethl, A. Gali, J. R. Maze, M. Atatüre, and C. Becher, Phys. Rev. Lett. **112**, 036405 (2014).
[17] V. Nadolinny, A. Komarovskikh, Y. Palyanov, I. Kupriyanov, Y. Borzdov, M. Rakhmanova, O. Yuryeva, and S. Veber, Phys. Status Solidi A **213**, 2623 (2016).
[18] W. F. Koehl, B. B. Buckley, F. J. Heremans, G. Calusine, and D. D. Awschalom, Nature (London) **479**, 84 (2011).
[19] V. A. Soltamov, A. A. Soltamova, P. G. Baranov, and I. I. Proskuryakov, Phys. Rev. Lett. **108**, 226402 (2012).
[20] D. J. Christle, P. V. Klimov, C. F. de las Casas, K. Szász, V. Ivády, V. Jokubavicius, J. Ul Hassan, M. Syväjärvi, W. F. Koehl, T. Ohshima, N. T. Son, E. Janzén, A. Gali, and D. D. Awschalom, Phys. Rev. X **7**, 021046 (2017).
[21] A. Batalov, V. Jacques, F. Kaiser, P. Siyushev, P. Neumann, L. J. Rogers, R. L. McMurtrie, N. B. Manson, F. Jelezko, and J. Wrachtrup, Phys. Rev. Lett. **102**, 195506 (2009).
[22] L. C. Bassett, F. J. Heremans, D. J. Christle, C. G. Yale, G. Burkard, B. B. Buckley, and D. D. Awschalom, Science **345**, 1333 (2014).
[23] M. L. Goldman, A. Sipahigil, M. W. Doherty, N. Y. Yao, S. D. Bennett, M. Markham, D. J. Twitchen, N. B. Manson, A. Kubanek, and M. D. Lukin, Phys. Rev. Lett. **114**, 145502 (2015).
[24] M. L. Goldman, M. W. Doherty, A. Sipahigil, N. Y. Yao, S. D. Bennett, N. B. Manson, A. Kubanek, and M. D. Lukin, Phys. Rev. B **91**, 165201 (2015).
[25] T. A. Abtew, Y. Y. Sun, B.-C. Shih, P. Dev, S. B. Zhang, and P. Zhang, Phys. Rev. Lett. **107**, 146403 (2011).
[26] K.-M. C. Fu, C. Santori, P. E. Barclay, L. J. Rogers, N. B. Manson, and R. G. Beausoleil, Phys. Rev. Lett. **103**, 256404 (2009).
[27] T. Plakhotnik, M. W. Doherty, and N. B. Manson, Phys. Rev. B **92**, 081203 (2015).
[28] R. Ulbricht, S. Dong, I.-Y. Chang, B. M. K. Mariserla, K. M. Dani, K. Hyeon-Deuk, and Z.-H. Loh, Nat. Commun. **7**, 13510 (2016).
[29] F. S. Ham, Phys. Rev. **138**, A1727 (1965).
[30] G. Kresse and J. Furthmüller, Phys. Rev. B **54**, 11169 (1996).
[31] P. E. Blöchl, Phys. Rev. B **50**, 17953 (1994).
[32] O. Bengone, M. Alouani, P. Blöchl, and J. Hugel, Phys. Rev. B **62**, 16392 (2000).
[33] A. Alkauskas, B. B. Buckley, D. D. Awschalom, and C. G. V. de Walle, New J. Phys. **16**, 073026 (2014).
[34] See Supplemental Material at http://link.aps.org/supplemental/10.1103/PhysRevB.96.081115 for details on the spin-orbit coupling calculations, dynamical Jahn-Teller theory and numerical results, calculated Huang-Rhys factors, and the estimated phonon overlap function.
[35] A. Gali, T. Demján, M. Vörös, G. Thiering, E. Cannuccia, and A. Marini, Nat. Commun. **7**, 11327 (2016).
[36] J. Heyd, G. E. Scuseria, and M. Ernzerhof, J. Chem. Phys. **118**, 8207 (2003).
[37] A. V. Krukau, O. A. Vydrov, A. F. Izmaylov, and G. E. Scuseria, J. Chem. Phys. **125**, 224106 (2006).
[38] P. Deák, B. Aradi, T. Frauenheim, E. Janzén, and A. Gali, Phys. Rev. B **81**, 153203 (2010).
[39] S. Steiner, S. Khmelevskyi, M. Marsmann, and G. Kresse, Phys. Rev. B **93**, 224425 (2016).

[40] J. P. Perdew, K. Burke, and M. Ernzerhof, Phys. Rev. Lett. **77**, 3865 (1996).

[41] F. S. Ham, Phys. Rev. **166**, 307 (1968).

[42] I. Bersuker, *The Jahn-Teller Effect* (Cambridge University Press, 2006).

[43] I. Bersuker and V. Polinger, *Vibronic Interactions in Molecules and Crystals* (Springer Science & Business Media, 2012).

[44] P. Kehayias, M. W. Doherty, D. English, R. Fischer, A. Jarmola, K. Jensen, N. Leefer, P. Hemmer, N. B. Manson, and D. Budker, Phys. Rev. B **88**, 165202 (2013).

[45] We note that Ref. [33] obtained $S = 3.63$ for the ${}^3A_2 \rightarrow {}^3E$ optical transition at the same size of supercell at a C_{3v} configuration that was obtained by smearing the occupation of the e orbitals evenly in the ${}^3E$ excited state.